https://doi.org/10.5194/egusphere-2022-479
Preprint. Discussion started: 3 August 2022

On the use of IASI spectrally resolved radiances to test the EC-Earth climate model (v3.3.3) in clear-sky conditions

Stefano Della Fera[1,2], Federico Fabiano[3], Piera Raspollini[2], Marco Ridolfi[4], Ugo Cortesi[2], Flavio Barbara[2], and Jost von Hardenberg[5,6]

[1]Department of Physics and Astronomy, University of Bologna, Bologna, Italy
[2]Institute of Applied Physics, National Research Council (IFAC-CNR), Sesto Fiorentino (FI), Italy
[3]Institute of Atmospheric Sciences and Climate, National Research Council (ISAC-CNR) Bologna, Italy
[4]National Institute of Optics, National Research Council (INO-CNR), Sesto Fiorentino (FI), Italy
[5]Department of Environment, Land and Infrastructure Engineering, Politecnico di Torino, Torino, Italy
[6]Institute of Atmospheric Sciences and Climate, National Research Council (ISAC-CNR), Torino, Italy

Correspondence: Stefano Della Fera (stefano.dellafera@unibo.it)

Abstract.

The long-term comparison between simulated and observed spectrally resolved radiances can represent a stringent test for the direct verification and improvement of General Circulation Models (GCMs). From the mid of 2000s, stable hyperspectral observations of the Mid-Infrared region (667 to 2750 cm^{-1}) of the Earth emission spectrum have been provided by different sensors (e.g., AIRS, IASI and CrIS). In addition, the FORUM mission, selected to be the ninth ESA Earth Explorer mission, will measure, starting from 2027, the terrestrial radiation emitted to space at the top of the atmosphere (TOA) from 100 to 1600 cm^{-1} filling the observational gap in the far-infrared (FIR) region, from 100 to 667 cm^{-1}.

In this work, in anticipation of FORUM measurements, we compare existing IASI observations to radiances simulated on the basis of the atmospheric fields predicted by the EC-Earth GCM (version 3.3.3) in clear-sky conditions. In order to simulate spectra based on the atmospheric and surface state provided by the climate model, the radiative transfer model σ-IASI has been implemented in the Cloud Feedback Model Intercomparison Project (COSP) package. Therefore, on-line simulations provided by EC-Earth model equipped with the new COSP + σ-IASI module have been performed in clear-sky conditions with prescribed sea surface temperature and sea-ice cover, every 6 hours, over a timeframe consistent with the availability of IASI data.

Systematic comparisons between observed IASI MetOp-A L1C data and model outputs have been performed in 10 cm^{-1} spectral intervals, on global and regional scales, by distinguishing the surface type (land, sea). The long term analysis shows a warm bias of the climate model in the roto-vibrational water vapour bands and in the $\mathrm{CO_2}$ absorption band. These biases represent a strong evidence of a temperature bias of the model in the upper-troposphere and in the stratosphere, while a cold bias occurs over land.

https://doi.org/10.5194/egusphere-2022-479
Preprint. Discussion started: 3 August 2022

1 Introduction

The Outgoing Longwave Radiation (OLR) flux, defined as the radiance emitted at top of the atmosphere integrated over the solid angle and over the spectral range from 100 to about 3330 $\mathrm{cm^{-1}}$ (3 - 100 μm), is a key quantity controlling the Earth Radiation Budget, and its accurate representation in General Circulation Models (GCMs) is crucial to get reliable historical and future simulations. For this purpose, GCMs are regularly tuned by adjusting parameters related to sub-grid processes not explicitly represented in the model, to constrain the simulated OLR fluxes to observed values (Mauritsen et al., 2012; Hourdin et al., 2017) mainly provided by the Earth Radiation Budget Experiment (ERBE) (Barkstrom, 1984) and the more recent Cloud and Earth Radiant Energy System (CERES) mission (Loeb et al., 2018).

The availability of long-term measurements of radiative fluxes, extending over almost 40 years, makes them fundamental to assess the performance of GCMs. In this framework, Wild (2020) recently examined the radiative global budget of 40 state-of-the-art global climate models participating in the Coupled Model Intercomparison Project phase 6 (CMIP6) through a systematic comparison of broadband energy fluxes at surface and TOA with the CERES-EBAF dataset. The study has shown an important improvement of the CMIP6 models compared to the earlier model generations but also a persistent inter-model spread, with a standard deviation of 2.8 $\mathrm{Wm^{-2}}$ for the all-sky OLR and of 2.6 $\mathrm{Wm^{-2}}$ for OLR in clear sky conditions.

Despite the comparison of observed and simulated broadband fluxes provides fundamental information about the performance of climate models, as shown in this work, the detection of model biases is complicated by the spectral integration, which may mask compensation errors in the OLR estimation. Conversely, spectrally resolved OLR contains the signatures of greenhouse gases (GHG), water and clouds and monitoring its behaviour by comparison to satellite measurements, offers an unprecedented opportunity to identify biases in GCMs and attributing them to a specific portion of the spectrum (Kiehl and Trenberth, 1997) (see appendix A) and, thus, to a specific physical parameter.

The first measurements of spectrally resolved radiances from space date back to 1970s but only starting from the 2000s, long-term and stable hyperspectral observations became available with the key satellite missions of the Atmospheric Infrared Sounding (AIRS, 2002-present), the Infrared Atmospheric Sounder Interferometer (IASI, 2006-present) and the Cross-track Infrared Sounder (CrIS, 2011-present) (Brindley and Bantges, 2016). The large amount of data available from these sensors opened interesting perspectives for the intercomparisons of instrumental measurements and long-term analysis. Whitburn et al. (2020) computed OLR spectral fluxes starting from IASI radiances, using precalculated angular distribution models (ADMs), and compared IASI OLR integrated fluxes to CERES and AIRS broadband OLR products. Susskind et al. (2012) investigated the OLR interannual variability using AIRS data from 2002 to 2011 and compared the energy fluxes computed from spectrally resolved radiances to CERES broadband fluxes. In the same framework, Brindley et al. (2015) explored the interannual variability of spectrally resolved radiances at different spatial scales by exploiting 5 years of IASI/MetOp-A data. While the aforementioned instruments are able to provide accurate measurements of the entire Mid-Infrared portion of the spectrum, from 667 to 2500 $\mathrm{cm^{-1}}$ (4 - 15 μm), the FIR spectral range, from 100 to 667 $\mathrm{cm^{-1}}$ (15 - 100 μm), which accounts for at least half of the Earth's energy emitted to space (Harries et al.), still lacks of systematic measurements from satellite because of the intrinsic difficulties of development of the proper FIR technology (Palchetti et al., 2020). Planned for launch in 2027, the

https://doi.org/10.5194/egusphere-2022-479
Preprint. Discussion started: 3 August 2022

Far-Infrared Outgoing Radiation and Monitoring (FORUM) mission will fill this observational gap. FORUM will fly in loose formation with the IASI new generation (IASI-NG) on the MetOp-SG-1A satellite (Ridolfi et al., 2020) thus, for the first time from space, the two instruments will cover the whole Earth's emission spectrum. In anticipation of FORUM measurements, we use a climatology of IASI clear-sky radiances built from L1C data over the period 2008-2016.

In this way, we can analyze OLR radiances at TOA to inspect and evaluate the climatology of the EC-Earth climate model. In particular, we describe how a spectral comparison between simulated and observed OLR can provide detailed information on model biases in temperature and humidity at different atmospheric levels, representing an alternative and reliable way, in addition to retrieval products and reanalysis datasets, to verify climate models performance.

Thus, in order to simulate upwelling OLR radiances starting from the climate model atmosphere, the fast radiative transfer model (RTM) σ-IASI (Amato et al., 2002) has been implemented in the CFMIP Observation Simulator Package (COSP v.1.4.1) inside the EC-Earth GCM. On-line historical simulations with prescribed sea surface temperatures (SSTs) and sea ice extension (SIE) have been performed using COSP + σ-IASI in clear-sky conditions, in the MIR and FIR spectral regions, over the period 2008 - 2016, compatible with IASI available observations.

Using a similar approach, an existing negative bias in the OLR flux of about 4 $\mathrm{Wm^{-2}}$ in the AM2 GCM (Team et al., 2004), was investigated by Huang et al. (2006) by comparison of AIRS spectra to simulated radiances, and attributed to a water vapour transport deficiency of the model. In the same way, Huang et al. (2007) highlighted the existence of opposite-in-sign biases in water vapour and in $\mathrm{CO_2}$ spectral bands, which produce fortuitous cancellations of spectral errors in the computation of the total broadband fluxes in the AM2 GCM.

In this work, the comparison between observed and model spectral radiance climatologies is preferred over the comparison between the climatology of atmospheric profiles (from the model and retrieved by IASI measurements) for the following reasons. The retrieval of vertical profiles from measured upwelling spectral radiances is a strongly ill-conditioned inverse problem, therefore a priori profile estimates are always used to constrain the retrieval. The used a priori information causes both global biases and local systematic smoothing errors in the retrieved profiles (Rodgers, 2000), thus making tricky the comparison of climatologies of profiles derived from the model and from the inversion of spectral radiance measurements (Rodgers and Connor, 2003). In addition, the implementation of an online instrument simulator - able to provide spectrally resolved radiances starting from the climate model state - paves the way for the direct assimilation of future IASI-NG and FORUM observations in the model.

The paper is organized as follows. In Section 2, models and observations are presented and briefly described. In Section 2.3, we introduce the implementation of the RTM in the COSP package in EC-Earth climate model. In Section 3 we present the results obtained by the long-term comparison between EC-Earth and IASI, we discuss the analysis method by highlighting the limits and the difficulties of the model-observations comparison in clear-sky conditions and draw the conclusions. Finally, in appendix A, we recall the radiometric quantities used in the analysis.

https://doi.org/10.5194/egusphere-2022-479
Preprint. Discussion started: 3 August 2022

2 Data and Methods

2.1 Models

2.1.1 EC-Earth Climate Model

The EC-Earth climate model version 3.3.3 (Hazeleger et al. (2010), Döscher et al. (2021), http://www.ec-earth.org) is a state-of-the-art, high-resolution Earth-system model participating in the last intercomparison project (CMIP6) (Eyring et al., 2016). EC-Earth includes advanced, robust and validated components for the atmosphere (the ECMWF IFS model cy36r4), the ocean (NEMO 3.6, (Madec et al., 2017)), sea ice (LIM3, (Fichefet and Maqueda, 1997)) and land processes (H-Tessel, (Balsamo et al., 2009). The model has been tuned by minimizing the differences of radiative fluxes at TOA and at the surface with respect to the observed fluxes from the CERES-EBAF-Ed4.0 dataset (Döscher et al., 2021).

In this work, atmosphere-only historical simulations have been performed with prescribed Sea Surface Temperatures and Sea Ice Extension in the standard resolution TL255L91-ORCA1 used for CMIP6. In this configuration, the atmospheric model IFS is characterized by a horizontal resolution of approximately 80 km and uses 91 vertical layers (Döscher et al., 2021).

In order to extract spectrally resolved OLR radiances from EC-Earth, we implemented the σ-IASI radiative transfer model (RTM) (Amato et al., 2002) inside the COSP module (v 1.4.1), a simulator package able to map the climate model state into synthetic observations which are directly comparable to the measurements of the real instruments (Bodas-Salcedo et al., 2011). The current version of COSP implemented in EC-Earth includes simulators for passive sensors such as CLOUDSAT, ISCCP, MODIS and MISR and active sensors like CALIPSO. It also provides the interface for an old version (v. 9.1) of Radiative Transfer for Television and Infrared Observation Satellite (TIROS) Operational Vertical Sounder (RTTOV) which can be linked to the package.

2.1.2 The σ-IASI/FORUM Radiative Transfer Model

σ-IASI is a monochromatic RTM able to simulate up-welling infrared radiances at high resolution (0.01 cm^{-1}) which can be convolved with the Spectral Response Function (SRF) of any instrument. More specifically, it has been customized to simulate the measurements by IASI-NG and of the future FORUM instrument. For each atmospheric layer, absorbing gas and wavenumber in the 10 - 3000 cm^{-1} range, the optical depths are computed using polynomial parametrizations determined on the basis of accurate cross-sections computed by KLIMA, a validated line-by-line RTM developed at IFAC-CNR (Cortesi et al., 2014). The inputs to the σ-IASI RTM are the surface pressure and temperature, the surface spectral emissivity, the profiles of temperature, humidity and concentrations of 11 gases (O3, CO2, N2O, CO, CH4, SO2, HNO3, NH3, OCS, HDO, CF4) and the cloud parameters (cloud cover, ice and liquid water content, effective radius of ice and liquid particles). The radiative transfer calculations are then performed using 61 fixed pressure levels and on a fixed wavenumber grid with a step of 0.01 cm^{-1}. The radiative code is also able to compute Jacobians with respect to all the geophysical variables, including the cloud parameters. The σ-IASI RTM has been extensively validated against IASI measurements(Liuzzi et al., 2017), Aircraft based Measurements (NAST-I) (Grieco et al., 2007) and ground-based measurements (Serio et al., 2008).

https://doi.org/10.5194/egusphere-2022-479
Preprint. Discussion started: 3 August 2022

2.2 Observations

2.2.1 IASI

Part of the payload of the MetOp series of EUMETSAT polar-orbiting meteorological satellites (Edwards and Pawlak, 2000), IASI is composed of a Fourier Transform Spectrometer and of an associated Integrated Imaging Subsystem (IIS), a broadband radiometer with a high spatial resolution for the co-registration with the Advanced Very-High-Resolution Radiometer (AVHRR) (Blumstein et al., 2004). MetOp is characterized by a sun-synchronous orbit with equatorial crossing time at 9:30 a.m. and 21:30 p.m. local times. IASI has been providing continuous data since October 2006, when it was firstly launched aboard MetOp-A. It was followed by IASI-B (MetOp-B), launched in 2012 and IASI-C (MetOp-C), launched in 2018.

All the three IASI instruments cover the spectral range from 645 to 2760 cm^{-1} with a spectral resolution of 0.5 cm^{-1} and a spectral sampling of 0.25 cm^{-1}, for a total of 8461 spectral channels. In order to obtain a uniform global coverage, IASI acquires measurements by scanning its Field of Regard (FOR) across the orbit track, with viewing angles that range from nadir up to 48.3 degrees on either side of the satellite track. Angularly, each FOR has a dimension of about 3.3° x 3.3° which, on ground, corresponds to a footprint of about 50 x 50 km at nadir. For each FOR (30 in total for scan) the instrument simultaneously acquires 4 spectra, each with a Field of View (FOV) of about 12 km of diameter at nadir.

In this work, we consider IASI data from the Fundamental Climate Data Record (FCDR) of reprocessed Metop-A Level 1c product provided by EUMESAT through the European Weather Cloud (EWC) service. We build a monthly clear-sky radiance climatology on a global scale between 2008 and 2016. Firstly, we use the quality-flag (variable GQisFlagQual) available in the dataset to discard corrupted spectra. Then, among the 120 observed spectra of each scan across the satellite track, we only select those corresponding to the 8 pixels closest to the nadir view. Thus, the clear-sky spectra are detected by exploiting the cloud cover derived from the AVHRR (variable GEUMAVHRR1BCLDFRAC and GEUMAvhrr1BQual). In the same way, we distinguish the land/ocean ground surface through the information (variable GEUMAvhrr1BLandFrac) provided by the AVHRR.

2.2.2 CERES

In this work, we exploit the CERES_SYN1deg_Ed4A products to get information about the observed cloud cover field on a global scale. Among the various products, the dataset provides 1°-regional 3-hourly cloud coverage derived from MODIS and geostationary satellites.

The high temporal resolution of the product allows to easily find coincidences with IASI measurements and to analyze the large-scale atmospheric conditions where the IASI spectrum has been detected. As discussed in Section 3.2, this is useful for the analysis, since CERES data refer to an area (1° x 1°) of extension similar to the EC-Earth atmospheric resolution (0.7° x 0.7°). We also use the CERES Energy Budget and Filled (EBAF) dataset v.4.1 to estimate the observed clear-sky broadband fluxes.

https://doi.org/10.5194/egusphere-2022-479
Preprint. Discussion started: 3 August 2022

2.3 Implementation of the σ-IASI RTM in the EC-Earth climate model

We created a specific GCM-RTM interface inside the COSP module of the EC-Earth climate model in order to perform the radiative transfer calculations *online*, that is by passing instantaneous atmospheric fields on a global scale to the RTM with a time step of 6 hours.

In the radiative scheme of IFS, the spectral emissivity of the surface is assumed to be constantly equal to 0.99 outside the atmospheric window region (800 - 1250 cm^{-1}). Conversely, within this region the emissivity depends on 8 types of surface: open sea, sea ice, interception layer, low and high vegetation, exposed and shaded snow and bare ground. These emissivity values are interpolated to a regular wavenumber grid with steps of 10 cm^{-1}, in the range from 100 to 3000 cm^{-1} and supplied to the σ-IASI RTM. The surface pressure and surface temperature are directly supplied to σ-IASI, while the simulated temperature, humidity and gases concentration profiles are first interpolated to the fixed pressure grid used by σ-IASI . Carbon dioxide, methane and nitrous oxide concentrations are horizontally and vertically uniform, depending only on time. The ozone mixing ratio used in the model simulation is a function of pressure, latitude and time, as described in Fortuin and Langematz (1995). Finally, concentrations of the other trace gases required by σ-IASI (SO_2, CO, HNO_3, NH_3, OCS, HDO, CF_4) are not modeled in the IFS, thus they are extracted from the U.S. Standard Atmosphere of the Atmospheric Constituent Profiles dataset (Anderson et al., 1986).

In order to minimize the huge impact of the radiative code on the GCM computing performance, the Look-Up Tables (LUTs) of optical depths parametrization coefficients are allocated and loaded from file only once at the beginning of the simulation, stored, and deallocated at the end of the process. Moreover, the outgoing radiance is computed only once every 4 latitude x longitude grid points of the EC-Earth model, for a total of about 6000 simulated spectra every 6 hours. In order to limit the data storage required, the high resolution spectrum computed by σ-IASI is convolved with a 10 cm^{-1}-wide box function and sampled every 10 cm^{-1}. Since EC-Earth does not include variables with a spectral dimension, we stored the simulated spectra in new auxiliary 4D variables declared in the IFS grib code scheme, using the dimension corresponding to vertical model levels for the spectral channels. These simplifications allowed to strongly reduce the computational cost of the model run, passing from an initial value of 90000 core hours per simulated year (CHPSY) to 4000 CHPSY, which is comparable to the cost of the other simulators already present in COSP and about 8 times higher than an EC-Earth standard atmosphere-only simulation without COSP (about 500 CHPSY).

3 Results and Discussion

3.1 Sensitivity of a simulated OLR spectrum to atmospheric temperature and gas concentrations

In order to better correlate the differences between modelled and observed radiances to model biases, we first studied, for a reference tropical atmosphere, the sensitivity of the radiance computed with σ-IASI to model temperature and trace species concentration.

https://doi.org/10.5194/egusphere-2022-479
Preprint. Discussion started: 3 August 2022

Figure 1 shows a spectrum of OLR at the TOA simulated by σ-IASI in clear-sky conditions. The spectral ranges measured by IASI and FORUM are highlighted, together with the approximated spectral ranges of the atmospheric window regions and the main gas absorption bands, which are summarised in table 1.

The FIR region (from 100 - 667 cm^{-1}) is dominated by the signature of the rotational band of water vapour (blue shade), whose study will be consolidated with the help of future FORUM measurements (Brindley and Harries, 1998). In anticipation of FORUM measurements, we focus here on the MIR region of the spectrum measured by IASI (645 - 2760 cm^{-1}) from 2006 onward. In this region, the spectrum undergoes a strong absorption between 640 - 750 cm^{-1} due to CO_2. In more detail, in the core of CO_2 band (660 - 670 cm^{-1}), the atmosphere appears opaque from space and the radiance reaching TOA is originated from the stratosphere. On the contrary, in the wing of the CO_2 band measured by IASI (700 - 750 cm^{-1}) , the effective emission level is located in the middle- to upper- troposphere. From 800 to 950 cm^{-1} and from 1100 to 1250 cm^{-1} (red shades), the atmosphere is almost transparent and the radiance reaching the TOA mainly originates from the surface or the atmospheric layers closest to the surface. Other strong absorption bands are located between 980 and 1080 cm^{-1} (ozone, green shade), between 1200 and 1400 cm^{-1} (methane, pink shade) and between 1250 and 1350 cm^{-1} (nitrous oxide, grey shade). Finally, the roto-vibrational water vapour band, located between 1400 and 1850 cm^{-1}, is highlighted.

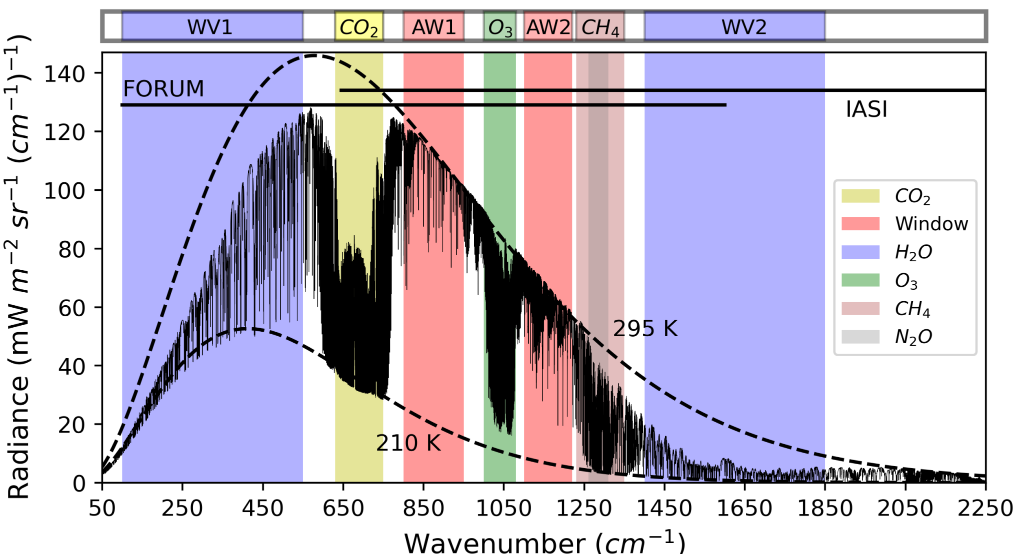

Figure 1. Spectrum simulated in clear-sky conditions over tropical ocean by the σ-IASI RTM. The main absorption bands are highlighted. Dashed lines show the equivalent blackbody emission at typical surface (295 K) and tropopause (210 K) temperatures.

The radiance reaching TOA originates mainly from upper atmospheric layers in the spectral regions of strong absorption, while in more transparent regions it originates from the lower atmospheric layers. More accurate information on the atmospheric layers contributing to the observed OLR spectrum can be extracted from the analysis of the Jacobians, defined as the partial derivatives of radiance with respect to the most relevant atmospheric parameters. The Jacobians in Figure 2 are com-

https://doi.org/10.5194/egusphere-2022-479
Preprint. Discussion started: 3 August 2022

Acronym	Band Details	Spectral Range (cm^{-1})
WV1	Water vapour (1)	100 - 500
CO_2	Carbon Dioxide	640 - 750
AW1	Atmospheric Window (1)	800 - 950
O_3	Ozone	980 - 1080
AW2	Atmospheric Window (2)	1100 - 1250
CH_4	Methane	1200 - 1400
N_2O	Nitrous Oxide	1250 - 1350
WV2	Water vapour (2)	1400 - 1850

Table 1. Approximated spectral intervals of the atmospheric windows and the main absorption bands highlighted in Fig. 1.

puted with the σ-IASI RTM for a tropical standard atmosphere over ocean at the IASI sampling of 0.25 cm^{-1} from 10 to 2250 cm^{-1}. For a better readability of the graph, the Jacobian values shown are the absolute values and normalized to their maximum value for each quantity, separately.

As we can see from Figure 2, the entire spectrum is sensitive to the temperature profile (red areas):

- the atmospheric window *AW1* is more transparent than the atmospheric window *AW2*, where the radiation is slightly sensitive to the water vapour concentration. In the first case (*AW1*), the radiation is affected by the temperature of atmospheric layers between 0 and 3 km while, in the second one (*AW2*), it is controlled by the temperature of layers at greater heights, up to about 7 km;
- the FIR is strongly affected by the temperature of lower and medium troposphere [3 - 10 km];
- the CO_2 absorption band is mainly sensitive to stratospheric temperature [25 - 40 km] in the core of the band and to mid-to-upper tropospheric temperature [5 - 20 km] in the wing of the band;
- the O_3 band is affected by surface, lower troposphere and lower stratosphere temperature;
- the roto-vibrational band of water vapour *WV2* is sensitive to tropospheric temperature [5 - 10 km].

Specific features can be noticed for each gas:

- the outgoing radiance between 1400 and 1850 cm^{-1} (*WV2*) is attenuated by H_2O in the upper troposphere (blue area) from 10 to 20 km. Water vapour also reduces OLR in the FIR region (*WV1*);
- between 980 and 1080 cm^{-1}, the ozone concentration strongly influences the spectrum over most of the troposphere (green area);
- at the same levels, the spectrum is affected by CH_4 concentration between 1200 and 1400 cm^{-1} and by N_2O between 1250 and 1350 cm^{-1};

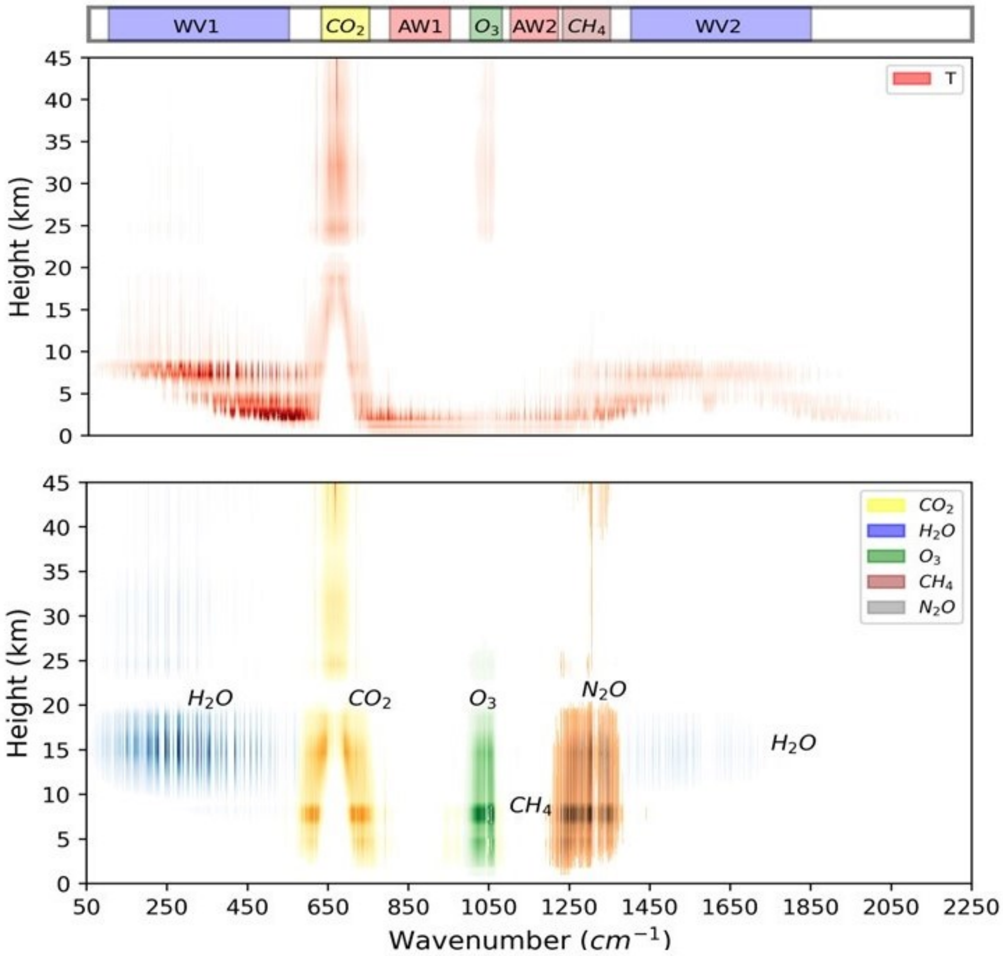

Figure 2. Absolute values of normalized Jacobians computed with σ-IASI for a tropical standard atmosphere with respect to the temperature (top panel) and gases concentration (bottom panel).

– in the CO_2 band, the spectrum is sensitive to CO_2 concentration at the same height where it is particularly sensitive to temperature profile. Thus, it is influenced by CO_2 concentration in the stratosphere in the core of the band while in the wings of the band it is sensitive to CO_2 present in the troposphere.

A change of sign of the Jacobian is observed for all gases between troposphere and stratosphere (not shown). In fact, in the troposphere absorption processes dominate the emission ones (so increased concentration reduces the OLR), while the opposite happens in the stratosphere.

https://doi.org/10.5194/egusphere-2022-479
Preprint. Discussion started: 3 August 2022

3.2 Model-Observation comparison strategy

An atmosphere-only historical simulation has been performed with the EC-Earth model coupled to σ-IASI RTM, as described in Section 2.3. The model was run with prescribed SSTs and SIE, using GHG concentrations, SST and SIE boundary conditions, from January 2008 to December 2016.

Due to the complication in comparing all-sky measurements at different resolutions, here we focus only on the clear-sky part, leaving the analysis of cloudy sky to a future work.

Generally, the radiative computation in clear-sky conditions in climate models exploits the same all-sky properties (e.g., surface temperature, temperature/humidity profile, surface albedo, aerosol), but with clouds removed. Since the temperature and humidity profiles of the model are indirectly affected by the presence of clouds, this causes a systematic negative bias when comparing observed and simulated clear-sky radiative fluxes. According to Sohn et al. (2006), this difference can reach up to -12 Wm^{-2} in the convectively active regions at tropical latitudes. In the CERES-EBAF 4.1 dataset, a new adjustment factor is introduced to generate TOA clear-sky fluxes that are more in line with the clear-sky fluxes represented in climate models, as described in Loeb et al. (2020) and in Loeb et al. (2018). On the contrary, in the EC-Earth vs IASI comparison, to mitigate this problem, we selected only the spectra computed over geographycal grid points where the simulated total cloud cover is less than 30%. This threshold allows to remove most humid grid points, while ensuring a good global coverage.

The selection of IASI spectra takes place in two different steps. Clear-sky spectra are first selected according to the cloud cover information provided by the AVHRR flying onboard MetOp-A. However, the resolution of the EC-Earth model, about 80 km at the equator, is very different from the spatial resolution of IASI, whose ground pixel is about 12 km near the nadir. This difference causes possible systematic errors, since the IASI filter of cloud cover reflects a smaller scale and is not comparable to the large-scale filter applied for the simulated radiances. Thus, to guarantee an "apple to apples" comparison, we applied an additional filter to IASI measurements by exploiting the observed large-scale total cloud cover field provided by CERES. This is provided every 3 hours by the CERES SYN1deg Ed4.1 dataset, whose grid point resolution (1° x 1°) is comparable to EC-Earth resolution. When a IASI clear-sky spectrum falls into a region where CERES cloud cover exceeds the 30% threshold, it is automatically discarded. This approach ensures consistency of the large-scale atmospheric conditions between simulated and observed outgoing radiances.

While the model outputs are provided every 6 hours on a fixed grid, MetOp performs about 14 orbits per day and IASI ground track is at 9:30 (descending node) and 21:30 local time (ascending node) at the equator. Therefore, the temporal and spatial consistence between IASI observations and model output is guaranteed by sampling observed and simulated spectra at corresponding local time and space. In fact, monthly means of observed and simulated outgoing radiances are computed over the same spatial grid by associating IASI measurements to the nearest EC-Earth grid-point. In order to limit the time mismatch between model and satellite measurements, IASI observations performed during the descending node (9:30 Local Solar Time equator crossing) are compared to EC-Earth synthetic radiances provided between 6 and 12 local time (day) while IASI observations performed during the ascending node (21:30 Local Solar Time equator crossing) are compared to EC-Earth synthetic radiances provided between 18 and 24 local time (night).

https://doi.org/10.5194/egusphere-2022-479
Preprint. Discussion started: 3 August 2022

3.3 Assessment of EC-Earth biases in simulated clear-sky radiances with respect to IASI measurements

On the basis of these assumptions, a systematic comparison has been performed using a dataset that covers the years from 2008 to 2016, for latitudes ranging from 60°S to 60°N. Land and ocean surface cases were analysed separately, however, here we focus only on the ocean cases. In fact, the low temporal sampling of the model (the RTM is called every 6 hours) and the uncertainties in the land surface emissivity do not allow to perform accurate comparisons between measured and observed radiances over land. In general, over land, the model shows a strong negative bias with respect to day-time measurements, and an important positive bias in night-time cases. Considering all-day measurements and simulations, a negative difference of about 3 K in brightness temperature persists in the atmospheric window between model and observations, pointing at a cold model bias of land surface temperature. Due to the significant differences in the atmospheric window, here we do not speculate on the results of the intercomparisons over land. We rather focus on the comparison of daytime measurements and model outputs over ocean.

Figure 3 shows the 9 years average of Brightness Temperature (BT) (see appendix A) differences (model - observations) over the ocean. Considering that model SSTs are constrained to be equal to the observed values, we expect small differences between model and IASI spectral radiances in the atmospheric spectral windows (*AW1, AW2*). Thus, the limited discrepancies in BTs obtained in the spectral window *AW1* in the tropical belt [30° S, 30° N] confirm the self-consistency of the comparison performed. Instead, as mentioned in Sec. 3.1, the atmospheric window *AW2* is more sensitive to the presence of water vapour and shows a small positive bias. At mid latitudes, however, especially in the southern hemisphere, a negative model bias is present in both the atmospheric windows, thus making difficult the comparison at all the frequencies at these latitudes. This model bias is thought to be linked to the cloud cover representation in the model and will be further discussed in Sect. 3.4.

Significant discrepancies, of about 3.5 K, are present in the CO_2 band at all latitudes, which might indicate a warm bias in the model temperature of the upper-troposphere and stratosphere. A warm bias is also seen in the roto-vibrational water vapour band (*WV2*) but this is limited to the Tropical latitudinal belt between 30°S and 30°N. In a similar way, the bias visible in the O_3 band is strictly dependent on latitude and is characterised by a positive sign at the tropics while it tends to take negative values at mid latitudes. As we observe the same pattern in the atmospheric window, we attribute this bias to the temperature of the atmospheric layers closest to surface (see Sect. 3.1).

On the basis of the above considerations, we focus our analysis on the discrepancies found over tropical ocean where the BT differences in the atmospheric windows are close to zero.

Figure 4 shows the 2008-2016 average of model simulated and observed BTs (equation A2) over ocean, at tropical latitudes [30° S, 30°N] (top panels) and their differences (bottom panels). In this case we see that the model is generally in good agreement with the observations and the most significant discrepancies are found in the CO_2 band, in the O_3 band and along the water vapour absorption band (*WV2*).

For the same period, the average clear-sky OLR flux computed by EC-Earth over ocean, between the latitudes 30°S and 30°N is equal to $288.47 \pm 0.34\ \mathrm{Wm^{-2}}$. This is slightly overestimated compared to the analogous average clear-sky flux obtained from CERES observations, that is equal to $287.36 \pm 0.32\ \mathrm{Wm^{-2}}$. From the Stefan-Boltzmann law, considering the power radiated

https://doi.org/10.5194/egusphere-2022-479
Preprint. Discussion started: 3 August 2022

by a black body at the temperature of 295 K (about the average surface temperature of tropical ocean), a difference of 1 Wm^{-2} corresponds to a BT difference of about 0.2 K, i.e. smaller than the biases localized in specific wavenumber ranges that we found from the spectral analysis. To date, systematic FIR spectral radiance measurements from space are not yet available, thus we are not able to characterize the discrepancies between model and observations in the whole OLR spectral range. Despite of that, the analysis presented shows clearly that a good agreement between simulated and observed total OLR fluxes may be obtained from the cancellation of opposite-in-sign systematic errors, localized in specific spectral ranges. In conclusion, observations of spectrally resolved OLR fluxes from space are needed for a proper tuning of model parameters.

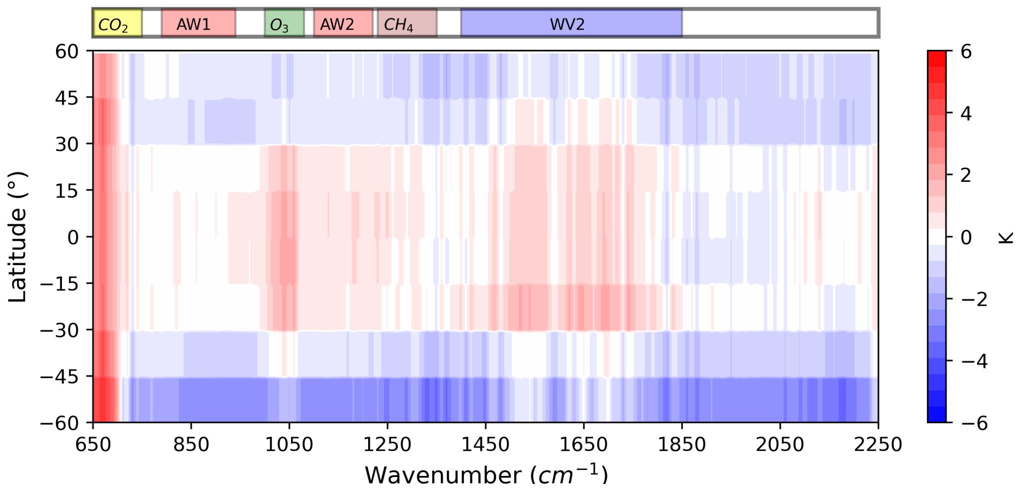

Figure 3. Brightness Temperature differences (model - observations) over ocean, averaged over the period 2008 - 2016

It is possible to characterise the height dependence of the model temperature bias by focusing the analysis on specific spectral bands, that are sensitive to the atmospheric temperature at different heights. The integral of the Jacobian of the temperature over height suggests that the largest sensitivity to temperature in the stratosphere is found in the spectral interval from 660 and 670 cm^{-1}, the highest sensitivity to temperature in the upper troposphere is found in the spectral interval from 700 and 710 cm^{-1}, and the maximum of the sensitivity in the mid-troposphere temperature is reached in the spectral interval from 730 and 740 cm^{-1}. As usual, the spectral channels in the atmospheric window, from 850 and 860 cm^{-1}, are a proxy of temperature of the lower troposphere and of surface (see Table 2).

Spectral range (cm^{-1})	660-670	700-710	730 - 740	850 - 860
Sensitivity Height (km)	[25-45]	[5-15]	[3-10]	[0-5]

Table 2. Spectral ranges and their sensitivity to temperature in specific altitude ranges.

As already mentioned, the spectral intervals 660 - 670 cm^{-1}, 700 - 710 cm^{-1} and 730 - 740 cm^{-1} are not only sensitive to temperature, they are also sensitive to $\mathrm{CO_2}$ concentration. The model, however, uses $\mathrm{CO_2}$ global average concentrations

https://doi.org/10.5194/egusphere-2022-479
Preprint. Discussion started: 3 August 2022

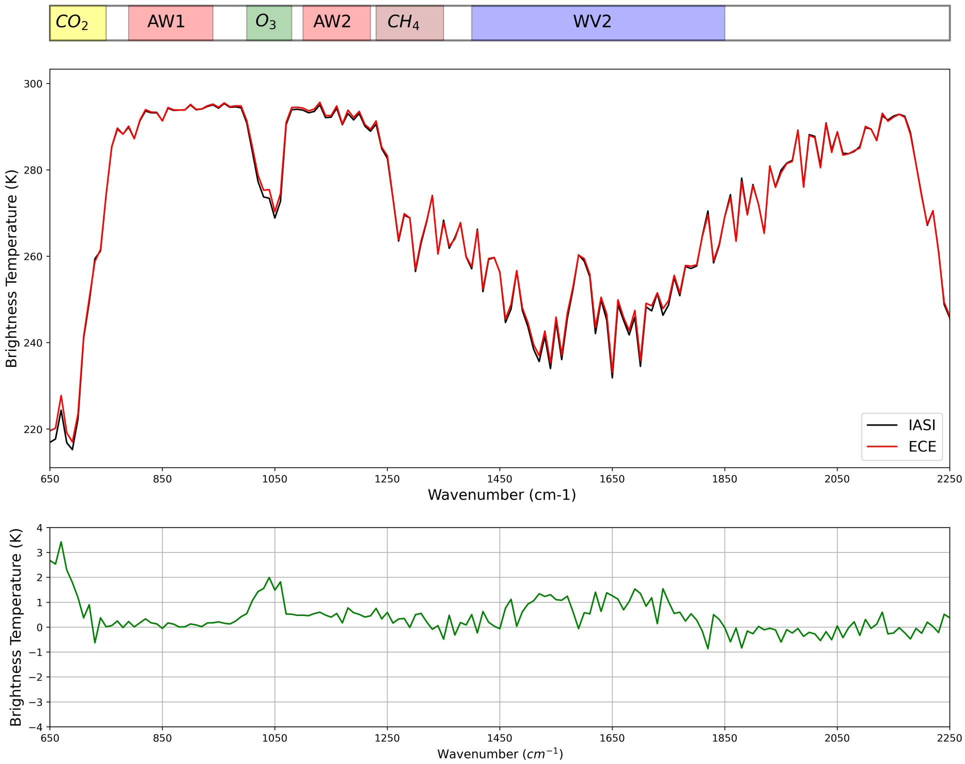

Figure 4. Average (2008-2016) Brightness Temperatures computed by EC-Earth and measured by IASI over the tropical ocean [30° S, 30°N] (top panel). The bottom panel shows the BT differences model minus observation.

smoothly increasing with time according to the actual measurements, thus any uniform warm model bias cannot be attributed to an erroneous carbon dioxide concentrations. The regional and seasonal variabilities of CO_2 concentrations amount at most to a few ppm, thus could cause only small local, seasonal biases.

On the basis of these considerations, we now consider Fig. 5, showing the 9-years monthly averages of simulated and observed BTs over ocean, for the selected spectral channels of Table 2.

Panel A of figure 5 confirms the presence of a strong stratospheric warm bias in the model. The more we move towards the lower layers of the atmosphere (panels A and B of Fig. 5), the more the bias is reduced, until its sign reverses in the spectral band 730 - 740 cm^{-1} (see panel C) which is sensitive to the mid-tropospheric temperature. Finally, as expected, the bias is very small in the atmospheric window over ocean (Panel D in figure 5) and the maximum BTs differences are always within 0.5 K. We notice that the seasonal cycle of the SST in EC-Earth is amplified, with a positive bias during the spring (MAM) and negative bias during the summer (JJA). The same pattern is observed in the other spectral channels of the atmospheric window *AW1* and is most likely due to the differences between the simulated and the observed cloud cover field (see Section 3.4) .

https://doi.org/10.5194/egusphere-2022-479
Preprint. Discussion started: 3 August 2022

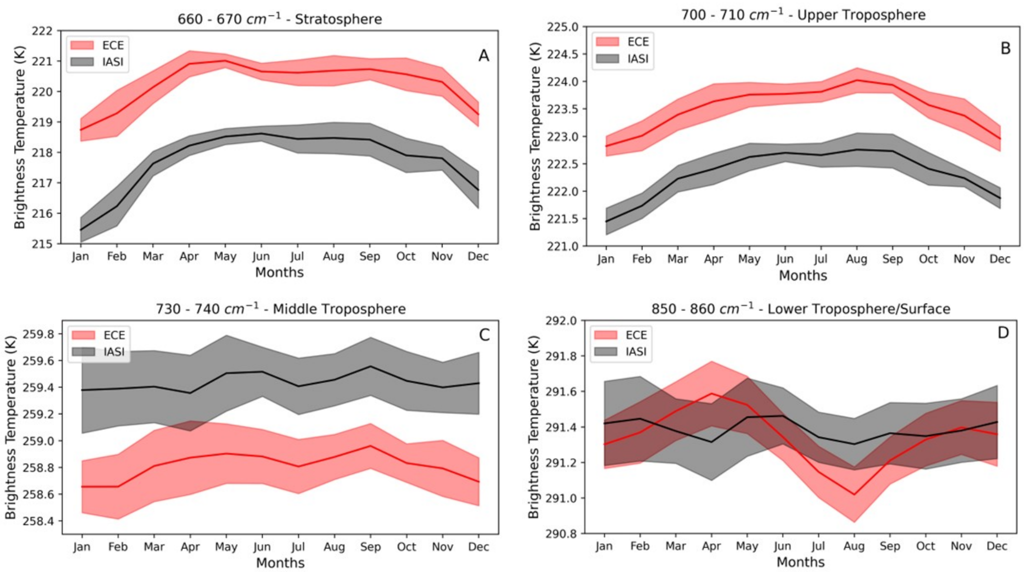

Figure 5. Brightness Temperature (BT) averaged in different spectral intervals over tropical ocean [30° S, 30°N]. The red line identifies the model BT while the black line describes the observed BT. The shadow areas represent the standard deviations. Note the different vertical scales used in the plots.

We now exploit the intervals 730 - 740 cm^{-1} and 1400 - 1410 cm^{-1} to explore the accuracy of the representation of the water vapour concentration in the model. In fact, as illustrated by the integrated, normalized jacobians reported on the left panel of Fig. 6, the spectral band 1400 - 1410 cm^{-1} (*WV2)* is sensitive both to the tropospheric temperature and to the upper tropospheric water vapour concentration. In both spectral intervals, the maximum sensitivity to temperature occurs between 3 and 10 km (green and pink lines on the left panel of Fig. 6). Since the previous analysis (panel C of Fig. 5) has shown a small negative BT bias in the channel 730 - 740 cm^{-1} assigned to a cold bias of the mid-tropospheric temperature in the model, if the water vapour concentration were well represented, we would see a negative BT bias in the spectral band 1400-1410 cm^{-1}. However, since the model BT in the channel 1400-1410 cm^{-1} shows a slightly positive bias (Figure 6, right panel), we conclude that the negative temperature bias of the model seems to be over-compensated by a dry bias of the water vapour profile in the 7 - 15 km range. In fact, a too dry upper troposphere in the model allows more radiant energy to reach the TOA, as also witnessed by the negative sign of the water Jacobian shown on the left panel of Fig. 6.

Finally, as in the $\mathrm{CO_2}$ case, EC-Earth uses local climatological monthly means of methane and ozone concentrations, thus, the discrepancies occurring in the ozone and methane absorption bands (not shown) most likely are due to biases of the simulated temperature.

https://doi.org/10.5194/egusphere-2022-479
Preprint. Discussion started: 3 August 2022

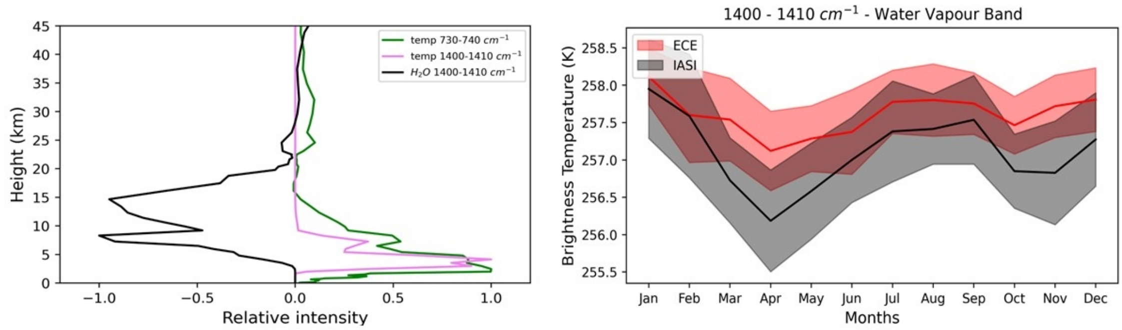

Figure 6. Left: Normalized Jacobians of temperature and water vapour integrated over the spectral band 1400 - 1410 cm^{-1} and 730 - 740 cm^{-1}. Right: Comparison of Brightness Temperature in the spectral band 1400 - 1410 cm^{-1}.

3.4 Discussion

We have seen that a perfect spatial and temporal matching of measurements and simulations is very difficult to actualise, therefore, systematic biases could also arise from the strategy adopted to sample the data. In order to evaluate the impact of the data sampling strategy, we carried out the following test. We interpolated the EC-Earth model cloud fraction and the measured CERES cloud fraction to a regular space grid of 1° x 1° and time step of 6 hours. Then, assuming alternatively the interpolated CERES and EC-Earth cloud fractions, we built the statistical distributions for the year 2008 of the same observed SST for the grid points with cloud fraction less than 30 %. Figure 7 shows the SST statistical distributions obtained for EC-Earth and CERES cloud fractions, at tropical- (left panel) and mid- (right panel) latitudes. At tropical latitudes the SST distributions obtained with the model (red boxes) and CERES (grey boxes) cloud fractions are quite similar: the average values differ by 0.4 K and the standard deviations ($\approx$ 4.5 K) differ by less than 0.1 K. On the other hand, at Southern mid-latitudes (-60° S, -45° S, see the right panel of Fig. 7) the offset between the two distributions amounts to 0.9 K. The small bias at the tropics could be related to the differences in the seasonal cycle we observed in the BT of the atmospheric spectral window (panel D of Figure 5). The larger bias of 0.9 K at the Southern mid-latitudes is likely contributing to the observed negative model BT bias found in the atmospheric window at the Southern mid-latitudes in Figure 3. The good agreement between the two SST distributions found in the tropical latitude belt strengthens our confidence on the previous analyses we presented for tropical latitudes. At these latitudes, the choice of comparing model and measured climatologies corresponding to cloud fractions smaller than 30 % ensures that the biases introduced by the data sampling strategy is smaller than $\approx$0.5 K, i.e. also smaller than most of the model biases inferred from Fig. 5.

We further tested the results of the spectral analysis by comparing the temperature and humidity obtained form the climate model outputs with data provided by ERA5, the latest climate reanalysis from ECMWF. The reanalysis combines available data from different instruments (satellites, ships, weather stations etc.) with models, to generate a complete and continuous global coverage of the main geophysical variables (Hersbach et al., 2020). The left panel of Fig. 8 shows the temperature differences

https://doi.org/10.5194/egusphere-2022-479
Preprint. Discussion started: 3 August 2022

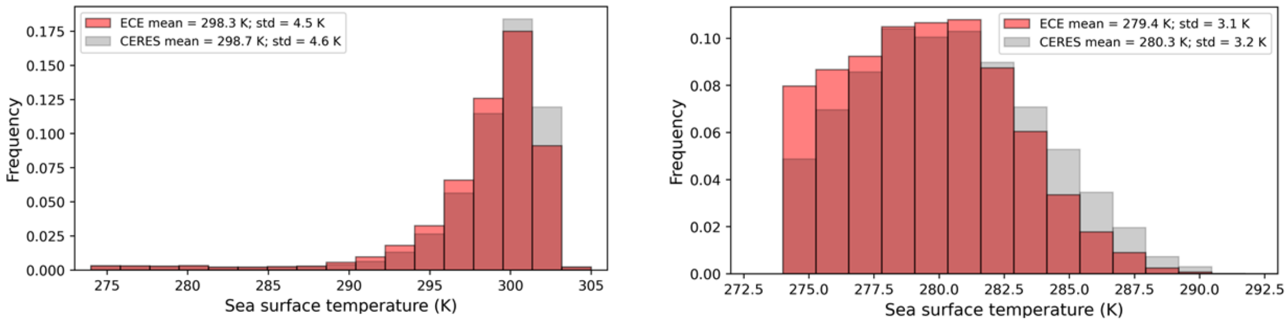

Figure 7. Distribution of sea surface temperature for cloud fraction < 30 %, assuming the EC-Earth (red) or the CERES (grey) cloud fractions. The distributions were computed for tropical- [-30 °S, + 30° N] latitudes (left) and mid- [-60 °S, - 45° S] latitudes (right).

between EC-Earth and ERA5 reanalysis, averaged over 15 years (2000 - 2014). The strong warm bias in the stratosphere confirms the discrepancy found in our spectral analysis in the region between 660 and 670 cm^{-1}. On the other hand, our spectral analysis did not detect the cold model bias visible in Fig. 8 at the tropopause. In fact, as shown in Fig. 2, the OLR spectrum is not very sensitive to temperature and gas concentrations at these heights. In addition, the spectral band from 700 to 710 cm^{-1} (see Table 2 and Panel B of Fig. 5) is partially affected by the positive stratospheric temperature bias, which can easily mask the underlying negative bias at the tropopause. We also note that the small negative model temperature bias present in the troposphere is consistent with the difference in BTs found in the spectral band from 730 to 740 cm^{-1} (panel C of Fig. 5).

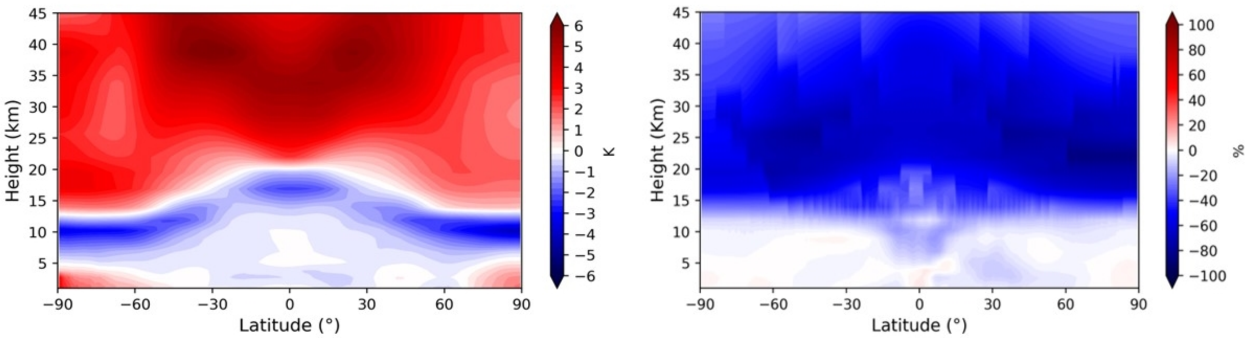

Figure 8. Differences betweeen EC-Earth climate model and ERA5 reanalysis temperatures (left) and percentage differences between EC-Earth climate model and ERA5 specific humidity. Differences are a 15 years [2000 - 2014] average.

The right panel of Fig. 8 shows the percentage differences between EC-Earth and ERA5 specific humidity, averaged over the period 2000-2014. The negative EC-Earth humidity bias found in the upper troposphere and stratosphere is consistent with

https://doi.org/10.5194/egusphere-2022-479
Preprint. Discussion started: 3 August 2022

the positive bias detected on the model simulated BTs in the spectral interval between 1400 and 1410 cm^{-1}. Indeed, the drier atmosphere of the model at these heights implies a greater amount of radiation reaching the TOA in the water vapour band.

4 Conclusion and future perspectives

In the measured spectral radiances, the signatures of the main climate variables can be identified, separated and used to assess climate model biases. This analysis can not be carried out on the basis of intercomparisons of total OLR fluxes that, as seen by the comparison of EC-Earth output and CERES observations, can easily hide compensating errors.

Thus, the availability of long-term measurements of spectrally resolved OLR radiances offers new important perspectives to strictly evaluate GCM performance. Indeed, the spectra measured on a global scale represent a more accurate benchmark than that provided by reanalysis datasets, which are computed using both observations and model simulations. In addition, the spectral analysis is not affected by the systematic biases affecting atmospheric profiles derived by applying a priori constraints to otherwise severely ill-conditioned inversions of satellite nadir spectral measurements.

We implemented the σ-IASI RTM in the COSP package in order to perform on-line simulations of synthetic clear-sky spectra starting from the EC-Earth GCM profiles on a global scale with a time step of 6 hours for the period 2008-2016. Thus, we compared the EC-Earth-simulated spectral radiances to the IASI-measured radiances built from the Fundamental Climate Data Record (FCDR) of reprocessed Metop-A Level 1c product on a frequency grid of 10 cm^{-1}. We limited the analysis to the clear-sky conditions identified by grid-points where the observed (CERES) and simulated (EC-Earth) cloud fraction is smaller than 30%. We found that such a small threshold limits the indirect effect of clouds on radiation in the model. The comparison has been firstly performed on a global scale ensuring the spatial and temporal coincidence between the modelled and observed spectra. Then, we focused on the day-time tropical ocean [30° S, 30°N] area, where the analysis is not affected by the uncertainties due to the land emissivity and the discrepancies between observed and simulated radiances in the atmospheric window are close to zero.

The spectral analysis carried out in this conditions leads to the detection of the following EC-Earth model biases which, due to compensations, do not show up in the comparison of the total OLR fluxes:

- A strong (≈3.5 K) positive temperature bias in the stratosphere.
- A small (≈1 K) negative temperature bias in the troposphere.
- A positive bias in the BTs in the water vapour band indicating an under-estimation of water vapour in the model in the upper troposphere.
- A negative bias of simulated BTs in the atmospheric window over land (of ≈3 K) suggests the existence of compensating errors in the total OLR flux.

Finally, we have shown that the results of our spectral analysis are consistent with those obtained by comparing EC-Earth temperature and specific humidity to the ERA5 reanalysis.

https://doi.org/10.5194/egusphere-2022-479
Preprint. Discussion started: 3 August 2022

The next phase of the work will involve the analysis of also spectral radiances in the presence of clouds, whose impact on the radiation represents the greatest source of uncertainty in climate models. The objective is to perform a spectral analysis of the cloud radiative effect and to detect the most important model biases by comparing climate model outputs to observations in all-sky conditions. Finally, the same approach could be extended to other climate models and, in the near future, it will involve FORUM FIR measurements for a comprehensive analysis of the climate model ability in reproducing the whole Earth emission spectrum.

Code availability. Permission to access the EC-Earth3 source code can be requested from the EC-Earth community via the EC-Earth website (http://www.ec-earth.org/, EC-Earth consortium, 2019a) and may be granted if a corresponding software license agreement is signed with ECMWF.

σ-IASI code is available upon request to its authors (http://www2.unibas.it/gmasiello/assite/as/sigma.html, e-mail: guido.masiello@unibas.it). Strictly confidential access to the σ-IASI code and to its interface to the climate model was granted for editors and reviewers, only for the purpose of evaluation of the present paper.

IASI data can be downloaded from EUMETSAT data center (https://www.eumetsat.int/eumetsat-data-centre).

Scripts and model data used for the analysis are available on Zenodo at https://doi.org/10.5281/zenodo.6912765

Appendix A: Brightness temperature and spectral OLR flux

The spectral radiance L_ν at wavenumber ν, can be converted into Brightness Temperature by using the inverse of the Plank function. Specifically, brightness temperature is defined as the temperature T_ν of the black-body B_ν that emits the same radiance L_ν at wavenumber ν. Thus we set:

$$L_\nu = B_\nu(T_\nu) = \frac{2hv^3c^2}{e^{\frac{hc\nu}{kT_\nu}} - 1} \tag{A1}$$

where h is the Planck's constant, c is the speed of light in vacuum and k the Boltzmann's constant. Inverting this formula we get:

$$T_\nu = \frac{hc\nu}{k\ln(1 + \frac{2hc^2\nu^3}{L_\nu})}. \tag{A2}$$

The spectral radiance is the energy flowing through the unit area, per unit time, per unit wavenumber and solid angle. In general, the spectral radiance is not isotropic, it usually depends on the orientation of the considered solid angle. This orientation can be identified using the zenith and the azimuth angles θ and ϕ, respectively. Thus, the spectral radiance, in general is a function $L_\nu(\theta, \phi)$. The spectral flux F_ν is defined as the integral of the radiance over an hemisphere of solid angle:

$$F_\nu = \int_\Omega L_\nu(\theta, \phi)\cos(\theta)d\Omega \tag{A3}$$

https://doi.org/10.5194/egusphere-2022-479
Preprint. Discussion started: 3 August 2022

where $d\Omega$ is the infinitesimal element of the solid angle Ω, the hemispheric domain of integration. In spherical coordinates we get $d\Omega = \sin(\theta)d\theta d\phi$. Thus, the spectral flux F_ν is written as:

$$F_\nu = \int_0^{2\pi} d\phi \int_0^{\pi/2} d\theta L_\nu(\theta,\phi)\cos(\theta)\sin(\theta) \tag{A4}$$

The total OLR flux is the integral of F_ν over the OLR spectral range, usually defined from 100 to 3333 cm^{-1} (or from 3 to 100 $\mu\mathrm{m}$ in wavelength).

Author contributions. SDF interfaced the σ-IASI radiative transfer model in the COSP package with the help of FF, MR and JVH. SDF and FF configured the climate model simulation and post-processed climate model data with the support of JVH. SDF developed the code to create the climatology of IASI measurements, with the help of UC, PR, FB and MR. SDF drafted the manuscript, and all authors contributed to its final version.

Competing interests. The authors declare that they have no conflict of interest

Acknowledgements. The authors acknowledge CINECA for proving computational resources through the Italian SuperComputing Resource Allocation (ISCRA, projects ECECOSP and ECEIASI) and EUMETSAT for making available the huge amount of L1c IASI data through the European Weather Cloud service (EWC). The σ-IASI RTM was made available by its authors in the frame of the "FORUM-scienza" (FORUM science) project, agreement No. 2019-20-HH.0, funded by the Italian Space Agency in the 2019-2022 time frame.

https://doi.org/10.5194/egusphere-2022-479
Preprint. Discussion started: 3 August 2022

References

Amato, U., Masiello, G., Serio, C., and Viggiano, M.: The σ-IASI code for the calculation of infrared atmospheric radiance and its derivatives, Environmental Modelling & Software, 17, 651–667, 2002.

Anderson, G. P., Clough, S. A., Kneizys, F., Chetwynd, J. H., and Shettle, E. P.: AFGL atmospheric constituent profiles (0.120 km), Tech. rep., Air Force Geophysics Lab Hanscom AFB MA, 1986.

Balsamo, G., Beljaars, A., Scipal, K., Viterbo, P., van den Hurk, B., Hirschi, M., and Betts, A. K.: A revised hydrology for the ECMWF model: Verification from field site to terrestrial water storage and impact in the Integrated Forecast System, Journal of hydrometeorology, 10, 623–643, 2009.

Barkstrom, B. R.: The earth radiation budget experiment (ERBE), Bulletin of the american meteorological society, 65, 1170–1185, 1984.

Blumstein, D., Chalon, G., Carlier, T., Buil, C., Hebert, P., Maciaszek, T., Ponce, G., Phulpin, T., Tournier, B., Simeoni, D., et al.: IASI instrument: Technical overview and measured performances, in: Infrared Spaceborne Remote Sensing XII, vol. 5543, pp. 196–207, SPIE, 2004.

Bodas-Salcedo, A., Webb, M., Bony, S., Chepfer, H., Dufresne, J.-L., Klein, S., Zhang, Y., Marchand, R., Haynes, J., Pincus, R., et al.: COSP: Satellite simulation software for model assessment, Bulletin of the American Meteorological Society, 92, 1023–1043, 2011.

Brindley, H. and Bantges, R.: The spectral signature of recent climate change, Current Climate Change Reports, 2, 112–126, 2016.

Brindley, H., Bantges, R., Russell, J., Murray, J., Dancel, C., Belotti, C., and Harries, J.: Spectral signatures of Earth's climate variability over 5 years from IASI, Journal of Climate, 28, 1649–1660, 2015.

Brindley, H. E. and Harries, J. E.: The impact of far IR absorption on clear sky greenhouse forcing: sensitivity studies at high spectral resolution, Journal of Quantitative Spectroscopy and Radiative Transfer, 60, 151–180, 1998.

Cortesi, U., Del Bianco, S., Gai, M., Laurenza, L. M., Ceccherini, S., Carli, B., Barbara, F., and Buchwitz, M.: Sensitivity analysis and application of KLIMA algorithm to GOSAT and OCO validation, Technical, scientific and research reports, 6, 1–153, 2014.

Döscher, R., Acosta, M., Alessandri, A., Anthoni, P., Arneth, A., Arsouze, T., Bergmann, T., Bernadello, R., Bousetta, S., Caron, L.-P., et al.: The EC-earth3 Earth system model for the climate model intercomparison project 6, Geoscientific Model Development Discussions, pp. 1–90, 2021.

Edwards, P. and Pawlak, D.: MetOp: The space segment for EUMETSAT's polar system, ESA bulletin, pp. 7–18, 2000.

Eyring, V., Bony, S., Meehl, G. A., Senior, C. A., Stevens, B., Stouffer, R. J., and Taylor, K. E.: Overview of the Coupled Model Intercomparison Project Phase 6 (CMIP6) experimental design and organization, Geoscientific Model Development, 9, 1937–1958, 2016.

Fichefet, T. and Maqueda, M. M.: Sensitivity of a global sea ice model to the treatment of ice thermodynamics and dynamics, Journal of Geophysical Research: Oceans, 102, 12 609–12 646, 1997.

Fortuin, J. P. and Langematz, U.: Update on the global ozone climatology and on concurrent ozone and temperature trends, in: Atmospheric Sensing and Modelling, vol. 2311, pp. 207–216, International Society for Optics and Photonics, 1995.

Grieco, G., Masiello, G., Matricardi, M., Serio, C., Summa, D., and Cuomo, V.: Demonstration and validation of the φ-IASI inversion scheme with NAST-I data, Quarterly Journal of the Royal Meteorological Society: A journal of the atmospheric sciences, applied meteorology and physical oceanography, 133, 217–232, 2007.

Harries, J., Brindley, H., Sagoo, P., and Bantges, R.: Coauthors, 2008: The far-infrared earth, Rev. Geophys, 46.

Hazeleger, W., Severijns, C., Semmler, T., Ştefănescu, S., Yang, S., Wang, X., Wyser, K., Dutra, E., Baldasano, J. M., Bintanja, R., et al.: EC-Earth: a seamless earth-system prediction approach in action, Bulletin of the American Meteorological Society, 91, 1357–1364, 2010.

Hersbach, H., Bell, B., Berrisford, P., Hirahara, S., Horányi, A., Muñoz-Sabater, J., Nicolas, J., Peubey, C., Radu, R., Schepers, D., et al.: The ERA5 global reanalysis, Quarterly Journal of the Royal Meteorological Society, 146, 1999–2049, 2020.

Hourdin, F., Mauritsen, T., Gettelman, A., Golaz, J.-C., Balaji, V., Duan, Q., Folini, D., Ji, D., Klocke, D., Qian, Y., et al.: The art and science of climate model tuning, Bulletin of the American Meteorological Society, 98, 589–602, 2017.

Huang, X., Ramaswamy, V., and Schwarzkopf, M. D.: Quantification of the source of errors in AM2 simulated tropical clear-sky outgoing longwave radiation, Journal of Geophysical Research: Atmospheres, 111, 2006.

Huang, Y., Ramaswamy, V., Huang, X., Fu, Q., and Bardeen, C.: A strict test in climate modeling with spectrally resolved radiances: GCM simulation versus AIRS observations, Geophysical Research Letters, 34, 2007.

Kiehl, J. T. and Trenberth, K. E.: Earth's annual global mean energy budget, Bulletin of the American meteorological society, 78, 197–208, 1997.

Liuzzi, G., Masiello, G., Serio, C., Meloni, D., Di Biagio, C., and Formenti, P.: Consistency of dimensional distributions and refractive indices of desert dust measured over Lampedusa with IASI radiances, Atmospheric Measurement Techniques, 10, 599–615, 2017.

Loeb, N. G., Doelling, D. R., Wang, H., Su, W., Nguyen, C., Corbett, J. G., Liang, L., Mitrescu, C., Rose, F. G., and Kato, S.: Clouds and the earth's radiant energy system (CERES) energy balanced and filled (EBAF) top-of-atmosphere (TOA) edition-4.0 data product, Journal of Climate, 31, 895–918, 2018.

Loeb, N. G., Rose, F. G., Kato, S., Rutan, D. A., Su, W., Wang, H., Doelling, D. R., Smith, W. L., and Gettelman, A.: Toward a consistent definition between satellite and model clear-sky radiative fluxes, Journal of Climate, 33, 61–75, 2020.

Madec, G., Bourdallé-Badie, R., Bouttier, P.-A., Bricaud, C., Bruciaferri, D., Calvert, D., Chanut, J., Clementi, E., Coward, A., Delrosso, D., et al.: NEMO ocean engine, 2017.

Mauritsen, T., Stevens, B., Roeckner, E., Crueger, T., Esch, M., Giorgetta, M., Haak, H., Jungclaus, J., Klocke, D., Matei, D., et al.: Tuning the climate of a global model, Journal of advances in modeling Earth systems, 4, 2012.

Palchetti, L., Brindley, H., Bantges, R., Buehler, S., Camy-Peyret, C., Carli, B., Cortesi, U., Del Bianco, S., Di Natale, G., Dinelli, B., et al.: unique far-infrared satellite observations to better understand how Earth radiates energy to space, Bulletin of the American Meteorological Society, 101, E2030–E2046, 2020.

Ridolfi, M., Del Bianco, S., Di Roma, A., Castelli, E., Belotti, C., Dandini, P., Di Natale, G., Dinelli, B. M., C-Labonnote, L., Palchetti, L., et al.: FORUM Earth Explorer 9: Characteristics of Level 2 Products and Synergies with IASI-NG, Remote Sensing, 12, 1496, 2020.

Rodgers, C. D.: Inverse methods for atmospheric sounding: theory and practice, no. 2 in Series on atmospheric, oceanic and planetary physics, World Scientific, Singapore, 2000.

Rodgers, C. D. and Connor, B. J.: Intercomparison of remote sounding instruments, Journal of Geophysical Research: Atmospheres, 108, 2003.

Serio, C., Masiello, G., Esposito, F., Di Girolamo, P., Di Iorio, T., Palchetti, L., Bianchini, G., Muscari, G., Pavese, G., Rizzi, R., et al.: Retrieval of foreign-broadened water vapor continuum coefficients from emitted spectral radiance in the H 2 O rotational band from 240 to 590 cm-1, Optics Express, 16, 15 816–15 833, 2008.

Sohn, B.-J., Schmetz, J., Stuhlmann, R., and Lee, J.-Y.: Dry bias in satellite-derived clear-sky water vapor and its contribution to longwave cloud radiative forcing, Journal of climate, 19, 5570–5580, 2006.

Susskind, J., Molnar, G., Iredell, L., and Loeb, N. G.: Interannual variability of outgoing longwave radiation as observed by AIRS and CERES, Journal of Geophysical Research: Atmospheres, 117, 2012.

https://doi.org/10.5194/egusphere-2022-479
Preprint. Discussion started: 3 August 2022

Team, G. G. A. M. D., Anderson, J. L., Balaji, V., Broccoli, A. J., Cooke, W. F., Delworth, T. L., Dixon, K. W., Donner, L. J., Dunne, K. A., Freidenreich, S. M., et al.: The new GFDL global atmosphere and land model AM2–LM2: Evaluation with prescribed SST simulations, Journal of Climate, 17, 4641–4673, 2004.

Whitburn, S., Clarisse, L., Bauduin, S., George, M., Hurtmans, D., Safieddine, S., Coheur, P. F., and Clerbaux, C.: Spectrally resolved fluxes from IASI data: Retrieval algorithm for clear-sky measurements, Journal of Climate, 33, 6971–6988, 2020.

Wild, M.: The global energy balance as represented in CMIP6 climate models, Climate Dynamics, 55, 553–577, 2020.